Theoretical Modeling and Experimental High-Speed Imaging of Elongated Vocal Folds

Yu Zhang*, Michael F. Regner, and Jack J. Jiang

***Abstract*—In this paper, the role of vocal fold elongation in governing glottal movement dynamics was theoretically and experimentally investigated. A theoretical model was first proposed to incorporate vocal fold elongation into the two-mass model. This model predicted the direct and nondirect components of the glottal time series as a function of vocal fold elongation. Furthermore, high-speed digital imaging was applied in excised larynx experiments to visualize vocal fold vibrations with variable vocal fold elongation from −10% to 50% and subglottal pressures of 18- and 24-cm H_2O. Comparison between theoretical model simulations and experimental observations showed good agreement. A relative maximum was seen in the nondirect component of glottal area, suggesting that an optimal elongation could maximize the vocal fold vibratory power. However, sufficiently large vocal fold elongations caused the nondirect component to approach zero and the direct component to approach a constant. These results showed that vocal fold elongation plays an important role in governing the dynamics of glottal area movement and validated the applicability of the proposed theoretical model and high-speed imaging to investigate laryngeal activity.**

***Index Terms*—Glottal area, high-speed digital imaging, two-mass model, vocal fold elongation.**

I. Introduction

VOCAL fold oscillation responsible for voice is the complex result of aerodynamic, physiological, and biomechanical properties of the larynx [1]. Laryngeal pathology is often associated with abnormal characteristics of glottal movements, such as incomplete glottal closure or reduced vibratory amplitude. Understanding glottal area characteristics of the larynx during phonation is crucial for understanding phonatory function and may be useful in assessing laryngeal health. A direct measurement method of the glottal area is through the use of high-speed digital video recording. Westphal and Childers [2] showed that high-speed imaging could be used to capture vocal fold motion. Lohscheller *et al*. [3] analyzed the pathological laryngeal dynamics by mapping high-speed images of vocal fold vibrations into 2-D diagrams. Yan *et al*. [4] applied automatic tracing of vocal fold movement to extract the glottal area of normal subjects. High-speed imaging has also been previously applied to estimate the parameters of the two-mass vocal fold model [5]–[7]. Recent studies have demonstrated the successful application of high-speed imaging in excised larynx experiments [8]. In this setup, experimental parameters such as subglottal pressure and vocal fold elongation can be systematically monitored and conveniently manipulated to control phonation.

The two-mass vocal fold model [9] represents a simple but effective way to capture the primary vibratory characteristics of vocal folds, and has been successfully used to simulate nonlinear vibratory dynamics in laryngeal pathologies [9]–[12]. Many phenomena, such as the phase difference between the superior and inferior edge of the vocal fold, bifurcations, and chaos, can be modeled in this theoretical system [10], [11]. However, most of the traditional two-mass models have neglected the impact of longitudinal stress on vibrations [9]–[12]. Vibration becomes more complicated when vocal fold elongation is considered and the nonlinear strain–stress relationship is included. Elongation is expected to be correlated with the prephonatory glottal width and vocal fold length. In addition, vocal fold tissue consists of a network of elastin fibers loosely organized in the superficial lamina propria and longitudinally parallel in the intermediate lamina propria [13], [14]. As vocal fold elongation increases, the tension and stiffness of these proteins may increase, which may result in a decrease in the amplitude of glottal area. Thus, the vocal fold models that include elongation are important to investigate the effect of longitudinal elongation in controlling voice production.

In this paper, we employ vocal fold modeling and excised larynx experiments to study the influence of vocal fold elongation on laryngeal activity during phonation. A theoretical model of vocal fold elongation is proposed to investigate the vibratory dynamics of vocal folds. In order to explore the theoretical predictions in an experimental model, measurements from 13 excised canine larynges including the glottal area were recorded using high-speed digital imaging during different subglottal pressure and elongation conditions. The direct and nondirect components were derived from the glottal area time series. The theoretical model simulations and experimental observations were then compared using these two parameters.

Manuscript received August 5, 2010; revised October 25, 2010; accepted November 10, 2010. Date of publication November 29, 2010; date of current version September 21, 2011. This work was supported in part by the Institute of Deafness and Other Communication Disorders under NIH Grant R01 DC005522-09. *Asterisk indicates the corresponding author.*

*Y. Zhang is with the Laboratory of Underwater Acoustic Communication and Marine Information Technology of the Ministry of Education, College of Oceanography and Environmental Science, Xiamen University, Xiamen 361005, China (e-mail: yuzhang@xmu.edu.cn).

M. F. Regner and J. J. Jiang are with the Department of Surgery, Division of Otolaryngology-Head and Neck Surgery, University of Wisconsin-Madison School of Medicine and Public Health, Madison, WI 53792 USA (e-mail: mfregner@wisc.edu; jjjiang@wisc.edu).

Color versions of one or more of the figures in this paper are available online at http://ieeexplore.ieee.org.

Digital Object Identifier 10.1109/TBME.2010.2095012

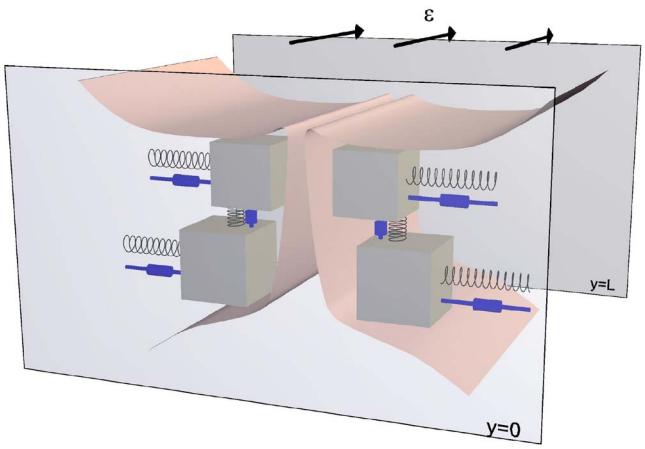

Fig 1. Schematic diagram of the two-mass model of vocal folds with elongation.

II. Theoretical Model Simulation of Vocal Fold Elongation

Traditional two-mass models cannot describe the longitudinal elasticity caused by vocal fold elongation [9]–[12]. In this study, we will consider the longitudinal elongation in a modified two-mass model. A diagram of the theoretical model of the vocal folds with elongation is illustrated in Fig. 1, where the x-axis corresponds to the lateral displacement and the y-axis corresponds to the anterior–posterior longitudinal deformation. The posterior side at $y = 0$ is fixed, and the anterior side receives an elongation ε and causes the glottal length to be $L = L_0(1 + \varepsilon)$ [15], where L_0 represents the initial glottal length without elongation. The point $y = L$ is fixed as a boundary.

Assuming symmetry between the vocal folds, the vibratory dynamic equations can be described as follows:

$$\begin{aligned} &m_1\ddot{x}_1 + r_1\dot{x}_1 + k_1(\varepsilon)(x_1 + \eta_{1k}x_1^3) \\ &\quad + \Theta(-a_1)c_1(\varepsilon)\left[\frac{a_1}{2l} + \eta_{1h}\left(\frac{a_1}{2l}\right)^3\right] \\ &\quad + k_c[(x_1 - x_2) + \eta_{ck}(x_1 - x_2)^3] = ldP_1 \qquad \text{(1a)} \\ &m_2\ddot{x}_2 + r_2\dot{x}_2 + k_2(\varepsilon)(x_2 + \eta_{2k}x_2^3) \\ &\quad + \Theta(-a_2)c_2(\varepsilon)\left[\frac{a_2}{2l} + \eta_{2h}\left(\frac{a_2}{2l}\right)^3\right] \\ &\quad + k_c[(x_2 - x_1) + \eta_{ck}(x_2 - x_1)^3] = 0 \qquad \text{(1b)} \end{aligned}$$

where x_1 and x_2 are the lateral displacements of the lower (m_1) and upper (m_2) parts of the vocal folds. k_i ($i = 1, 2$) is the stiffness constant of the mass m_i. Two masses m_1 and m_2 are vertically coupled by a linear spring with a constant coupling stiffness k_c. r_i is the damping constant. d_i is the thickness of the mass m_i. $a_1 = a_0 + 2Lx_1$ and $a_2 = a_0 + 2Lx_2$ are the lower and upper glottal areas, respectively. Assuming an initially rectangular (nondiverging and nonconverging) glottis, a_0 is the initial glottal area. During glottal closure, two sides of the vocal folds will collide with each other and produce the nonlinear restoring force $\Theta(-a_i)c_i\left[(a_i/2l) + \eta_{ih}(a_i/2l)^3\right]$ [9] where $c_i = 3k_i$ is the additional collision stiffness and the collision function $\Theta(x)$ can be described as [10]

$$\Theta(x) = \begin{cases} \tanh(50x/x_0), & x > 0 \\ 0, & x \le 0. \end{cases} \qquad (2)$$

The pressures and glottal airflow from the subglottal region to the minimum glottal area in the vertical axis satisfy the Bernoulli equation. The driving pressure P_1 is then

$$P_1 = P_s\left[1 - \Theta(a_{\min})\left(\frac{a_{\min}}{a_1}\right)^2\right]\Theta(a_1) \qquad (3)$$

and the minimal glottal area $a_{\min}$ can be described as

$$a_{\min} = \min(a_1, a_2) \qquad (4)$$

In experiments, $a_{\min}$ as the minimum glottal gap in the vertical axis can be measured by using high-speed imaging. For the periodic time series $a_{\min}$ with fundamental period T, its Fourier series of the time series can be expanded as

$$a_{\min}(t) = \bar{a} + \sum_{\substack{k=-\infty \\ k\neq 0}}^{\infty} \tilde{a}_k e^{jk\omega_0 t} \qquad \text{(5a)}$$

$$\tilde{a}_k = \frac{1}{T}\int_T a_{\min}(t)e^{-jk\omega_0 t}dt \qquad \text{(5b)}$$

where ω_0 is the fundamental frequency satisfying $\omega_0 = 2\pi/T$. The coefficient $\bar{a}$ is the direct component corresponding to the average value of $a_{\min}$ over time:

$$\bar{a} = \frac{1}{T}\int_T a_{\min}(t)dt. \qquad (6)$$

The coefficient $\tilde{a}_k$ as the kth harmonic component corresponds to the nondirect component. Considering the orthogonal property of $e^{jk\omega_0 t}$, from (5), we then have the following nondirect component:

$$\tilde{a} = \sqrt{\sum_{k=-\infty, k\neq 0}^{\infty} |\tilde{a}_k|^2} = \sqrt{\frac{1}{T}\int_T (a_{\min}(t) - \bar{a})^2\, dt}. \qquad (7)$$

Physically, the average total power $(1/T)\int_T a_{\min}^2(t)dt$ of the glottal area signal $a_{\min}$ equals the sum of the powers of the direct component $\bar{a}$ and nondirect component $\tilde{a}$. For static vocal folds ($x_i \to 0$), $\tilde{a}$ approaches zero and $a_{\min}$ approaches $\bar{a}$. An increase of $\tilde{a}$ increases the vocal fold vibratory power.

Vocal fold elongation produces a longitudinal stress σ_i that includes vocal fold body and cover stress components [16] and can be described as

$$\sigma_i = \frac{\sigma_{ib}D_{ib} + \sigma_{ic}D_{ic}}{D_{ib} + D_{ic}} \qquad (8)$$

where σ_{ib} and σ_{ic} denote longitudinal body and cover stresses, and D_{ib} and D_{ic} denote body and cover depths. According to the experimentally measured stress–strain data of canine larynges by Alipour and Titze [13], σ_{ib} and σ_{ic} can be fitted using the exponential function as

$$\sigma_{ib} = \sigma_{ib0} + A_{ib}[\exp(B_{ib}\varepsilon) - 1] \qquad \text{(9a)}$$

$$\sigma_{ic} = \sigma_{ic0} + A_{ic}[\exp(B_{ic}\varepsilon) - 1] \qquad \text{(9b)}$$

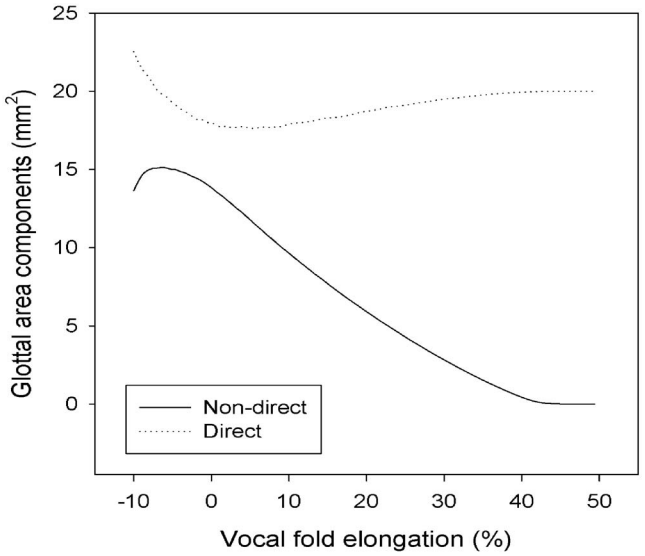

Fig. 2. Effects of vocal fold elongation on the nondirect component $\tilde{a}$ and the direct component $\bar{a}$ of glottal area from the two-mass model of the vocal folds with elongation.

where A_{ib}, B_{ib}, A_{ic}, and B_{ic} are the fitting parameters. σ_{ib0} and σ_{ic0} represent the initial body and cover stresses at $\varepsilon = 0$. The stress σ_i can be converted to stiffness k_i by equating the expressions for fundamental frequency of a vibrating string and a mass, $F_0 = (1/2\pi)\sqrt{k_i/m_i} = (1/2L)\sqrt{\sigma_i/\rho}$ [15]. Thus, the stiffness constant k_i is

$$k_i = k_{i0} + \frac{\pi^2 D_i d_i}{L}\left\{\frac{D_{ib}A_{ib}}{D_{ib}+D_{ic}}[\exp(\varepsilon)-1] + \frac{D_{ic}A_{ic}}{D_{ib}+D_{ic}}[\exp(\varepsilon)-1]\right\} \quad (10)$$

where $k_{i0} = (\pi^2 D_i d_i/L)\{D_{ib}\sigma_{ib0}/(D_{ib}+D_{ic}) + D_{ic}\sigma_{ic0}/(D_{ib}+D_{ic})\}$ represents the initial stiffness of the mass m_i at $\varepsilon = 0$. From (1) to (10), we can investigate the dynamics of the vocal folds with elongation. In particular, when $\varepsilon = 0$, this model reduces to the traditional two-mass vocal fold model without elongation [9]–[12].

The default values used by Ishizaka and Flanagan [9] were used in numerical calculations of the present model: $m_1 = 0.125$, $m_2 = 0.025$, $r_1 = r_2 = 0.02$, $k_{10} = 0.08$, $k_{20} = 0.008$, $k_c = 0.025$, $\eta_{ik} = 100$, $\eta_{ck} = 100$, $\eta_{ih} = 500$, $d_1 = 0.25$, $d_2 = 0.05$, $a_{01} = a_{02} = 0.1$, $l = 1.4$, and $\rho = 0.00113$. $D_{ib}/(D_{ib}+D_{ic}) = 0.7$ and $D_{ic}/(D_{ib}+D_{ic}) = 0.3$ were used according to the body-cover theory by Story and Titze [16]. The parameters $A_{ib} = 0.34$, $B_{ib} = 5.8$, $A_{ic} = 4.5$, and $B_{cb} = 3.47$ were used in order to make the model outputs of $\bar{a}$ and $\tilde{a}$ sufficiently approach the experimental measurements. These parameter values are within the range given by the study by Alipour and Titze [13]. All parameters are given in units of cm, g, ms, and their corresponding combinations. The results of the nondirect and direct components of glottal area from the two-mass model with elongation are illustrated in Fig. 2, where the subglottal pressure Ps is 18-cm H_2O. Note that these two components are functions of vocal fold elongation. A maximal value of $\tilde{a}$ can be found at a certain negative elongation. However, a sufficiently increased ε decreases $\tilde{a}$. Similar results can also been obtained when other values of A_{ib}, B_{ib}, $A_{\rm ic}$, and B_{cb} in the study by Alipour and Titze [13] were used.

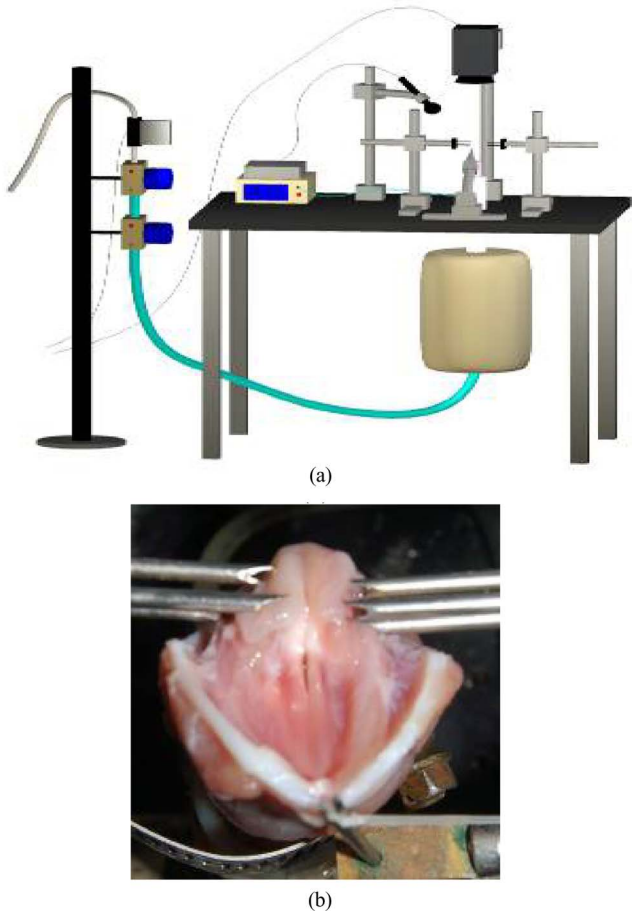

Fig. 3. (a) Excised larynx experimental system. (b) Sexcised canine larynx mounted in a physiologically phonating position.

III. Excised Larynx Experimentation

To investigate the direct and nondirect components of glottal area in an *in vitro* model, experiments were conducted with 13 excised canine larynges. Each canine larynx was mounted on an excised larynx phonation system, as illustrated in Fig. 3. The trachea was securely attached to the apparatus using a metal pull clamp. Lateral micromanipulators provided control of arytenoid adduction and an anterior micromanipulator was sutured to the laryngeal prominence of the thyroid cartilage to control elongation. Pressurized air from a building source was routed through two Concha Therm III humidifiers in series (Fisher & Paykel Healthcare Inc., Laguna Hills, CA), a pseudolung to simulate the capacitive and volumetric characteristics of the respiratory system, and the excised larynx. A mass pneumotachometer (model FMA-1601A; Omega Engineering Inc., Stamford, CT) and a manometer (Heise 901 series; Ashcroft Inc., Stratford, CT) recorded measurements of the air flow and pressure. A high-speed digital camera (Fastcam-ultima APX) recorded

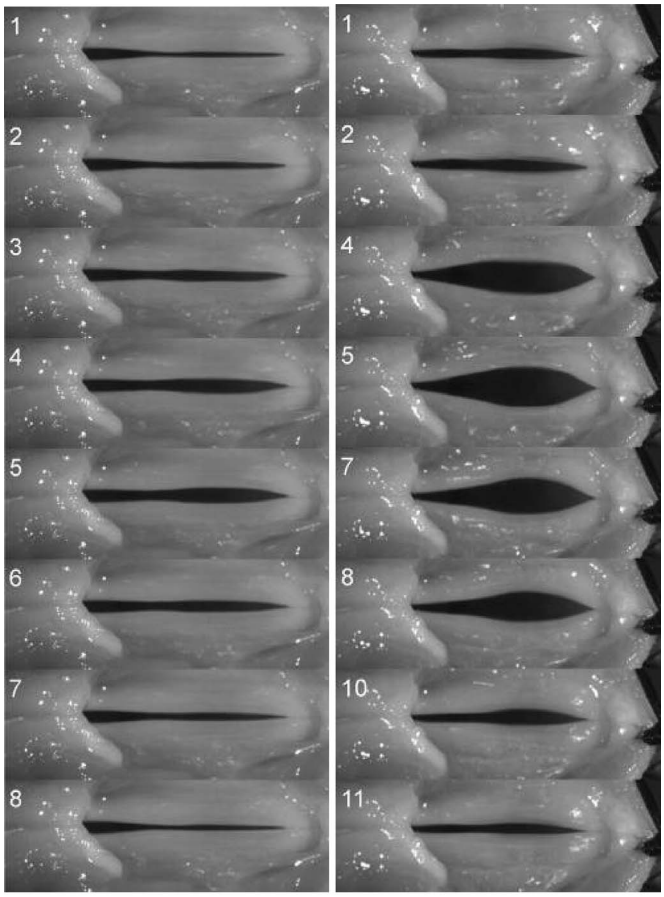

Fig. 4. High-speed image sequences of glottal area throughout a single glottal cycle of an excised canine larynx at (a) 20% vocal fold elongation and (b) –5% vocal fold elongation. Frame numbers are indicated in the upper left corner.

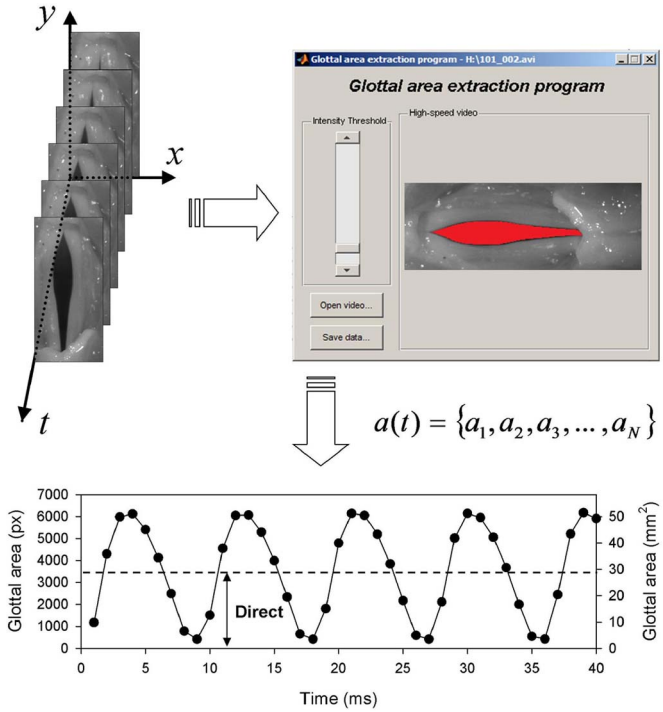

Fig. 5. Glottal area time series extracted from the high-speed imaging of glottal movements, where the lighting obtained after using image detection allows the glottal area to be clearly distinguished from the surrounding tissues.

video of vocal fold vibration at a sampling frequency of 4000 frames/s with a resolution of 256 × 512 pixels.

With the specimen mounted on the excised larynx phonation system, air pressure was increased until phonation began. The independent variables of the experiment were subglottal pressure and vocal fold elongation. Two subglottal pressure levels, 18-cm H_2O and 24-cm H_2O, were studied. The vocal fold length was measured with a digital caliper with accuracy of 0.1 mm. The mean glottal length of the 13 larynges at 0% elongation was 15.3 mm and the standard deviation (SD) was 1.5 mm. Thirteen vocal fold elongation levels were studied ranging from -10% to $+50\%$, with an elongation step size of 5%. The experiment followed a 2×13 factorial design. For a given subglottal pressure and elongation, 500 ms of phonation video was recorded by the high-speed digital camera. Example image sequences are depicted in Fig. 4, where (a) and (b) correspond to 20% and -5% vocal fold elongation, respectively. Clearly, -5% vocal fold elongation causes a larger vibratory amplitude and a more curved glottal shape than 20% elongation does. Because of the memory limitations of the high-speed digital camera, only two replicates were recorded per larynx and experimental condition. Thus, a total of 26 unique experimental conditions per larynx comprised the experimental database.

In order to extract the glottal area from the recorded high-speed images, we applied an image processing procedure by combining Lagrange interpolation analysis with Canny image edge detection as previously reported [17], [18]. In Fig. 5, the lighting of the laryngeal framework shows that the image detection method allows the glottis to be clearly distinguished from the surrounding vocal fold tissues. The periodic oscillations of the glottal area were acquired by using the image detection method. Therefore, applying this image detection procedure to the 2000 high-speed frames, we obtained the glottal area signal $a(t)$ as a function of time. The direct $\bar{a}$ and nondirect $\tilde{a}$ components of glottal area signal $a(t)$ were calculated. Experimental data are presented as means and SD over the 13 larynges. Graphs were produced using SigmaPlot 11.0 (Systat Software, Inc., San Jose, CA).

Fig. 6 shows the results from the experimental measurements in comparison with those from the theoretical model. 7000 pixels in each high-speed image correspond to the area of 60 mm^2. All measurements in pixels were converted using this landmark value. For 13 larynges, larger means and SD of $\bar{a}$ and $\tilde{a}$ can be found at low elongations. At -5% elongation, the maximal value of $\tilde{a}$ can be found. However, when ε is increased to 50%, $\tilde{a}$ sufficiently decreases and $\bar{a}$ approaches constants. The shape of the graphs of the direct and nondirect components of glottal area did not differ substantially between the experimental and theoretically derived data. The theoretical model simulations and experimental observations showed a better agreement at larger elongation.

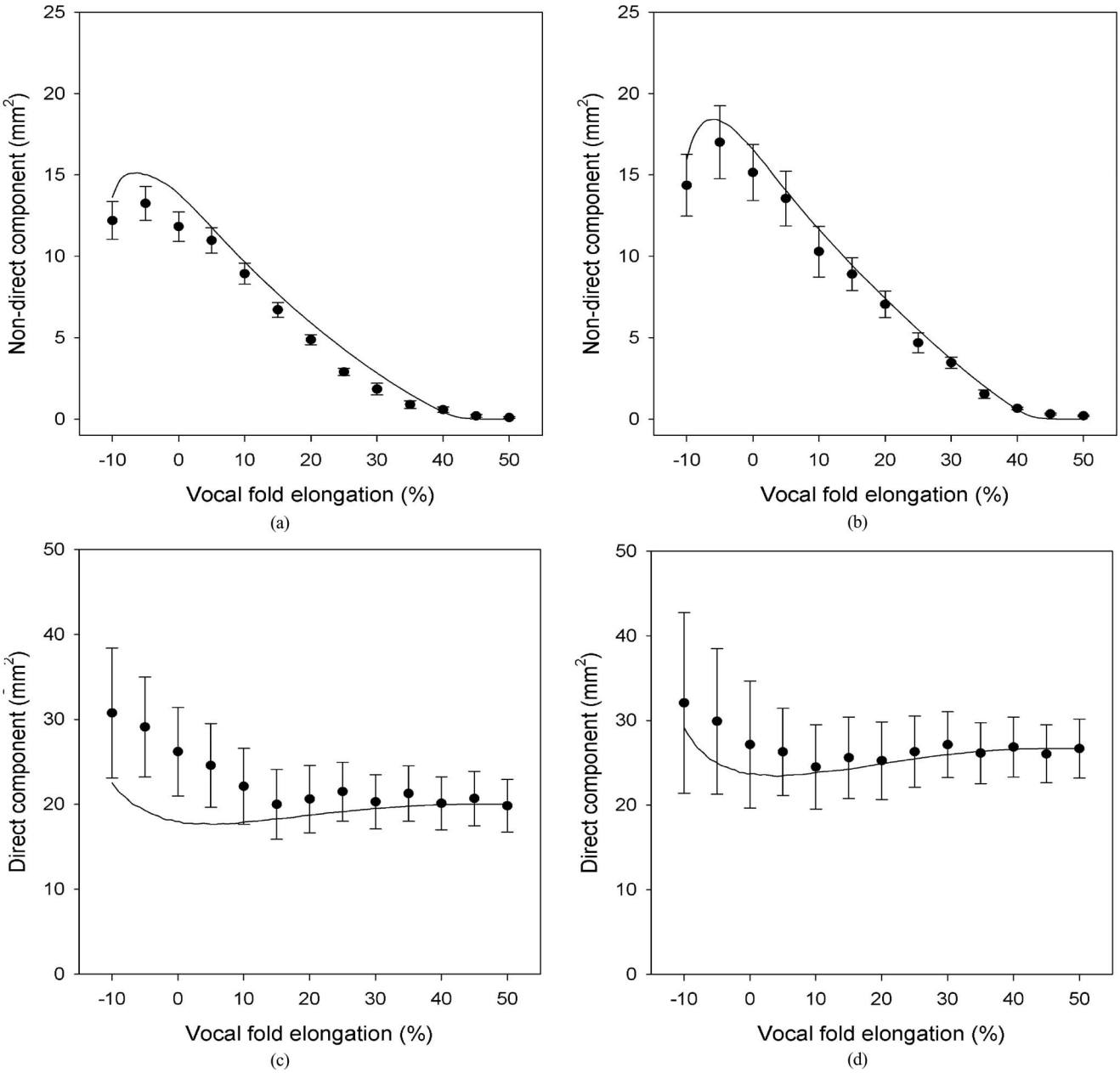

Fig. 6. Effects of elongation on the nondirect component $\tilde{a}$ from both theoretical and experimental data at (a) 18-cm H_2O and (b) 24-cm H_2O, and on the direct glottal area component $\bar{a}$ at (c) 18-cm H_2O, and (d) 24-cm H_2O. The solid line indicates the theoretical prediction, and the circles represent the experimental measurements. SD are indicated by whiskers.

IV. Discussion

In this study, a theoretical model of vocal fold vibration was proposed to incorporate previous measurements of vocal fold strain [13] into the mathematical model in order to investigation the effect of the elongation on phonation. Alipour and Titze [13] measured the elastic behaviors of canine vocal fold tissues, and conducted slow stretching and releasing experiments to obtain stress–strain data. The empirical exponential stress–strain relationship they reported was used in our vocal fold model to simulate the stress induced by large elongations. While previous traditional vocal fold models have included constant springs to simulate pathologies such as Parkinson's disease, vocal fold nodules, and polyps [9]–[12], they have ignored important covariants of vocal fold elongation such as the longitudinal tension and vocal fold length. There is a paucity of literature which provides an elongation treatment in vocal fold models. The proposed model in this study provides an effective approach to integrate the stress–strain relationships that have been empirically measured into the two-mass model. This is an important step in advancing model simulations of vocal fold elongation.

Recent research has investigated the possibility of modeling voice production using finite element models of the elongated vocal folds. Tao and Jiang [19] used a displacement boundary condition on the posterior cross-sectional plane to simulate elongation. Their results suggested that longitudinal elongation

affected tension distribution, longitudinal normal stress, maximum vibratory amplitude, and frequency. However, their model used a strictly linear stress–strain relationship, which is only applicable for low elongations ($\varepsilon < 15\%$) [19]. The results from Tao and Jiang are in good agreement with our model at small strains. In this study, we consider stress to be an exponential function of strain such that $\sigma \propto \exp(\varepsilon) - 1$. This allowed us to reliably model the vibratory dynamics of vocal folds in a much wider range of elongation. Because finite element models carry a large computational cost, low-dimensional models of the vocal folds with elongation are in this regard advantageous. Two-mass models also tend to be more easily applied because of their conceptually simplicity. However, the two-mass models cannot model the complex geometric shape of vocal folds [9], [10]. Such a limitation might contribute to the differences between the model simulation and experimental measurements at negative elongations where the curved glottal shapes become more significant (see Fig. 4). Extension of the two-mass models to multimass models [16] or 3-D models [14], [21] may represent a valuable solution for the simulation of curved vocal fold vibratory patterns under vocal fold elongation. Accordingly, it is important to recognize that the glottal area time series does not represent vocal fold motion in its entirety, but can characterize the motion of the upper and lower margins of the vocal folds.

Previous experimental studies have applied high-speed digital imaging to investigate the role of glottal area and its derivative parameters in phonation [4], [20], [21]. High-speed imaging has also been applied to estimate asymmetric vocal fold model parameters of normal subjects and patients [5], [7]. But none have reported studying the direct and nondirect components of glottal area under vocal fold elongation directly. Few direct comparisons between theoretical model glottal area parameters and real system glottal area parameters have been performed. In this study, high-speed imaging provides glottal area information with high temporal and spatial resolution under a variety of elongation conditions, as shown in Fig. 4. Comparisons of the nondirect components $\tilde{a}$ between our model simulations and high-speed imaging measurements under different elongations showed good qualitative agreement, as shown in Fig. 6. In comparison to the direct component, the nondirect component of glottal area is more sensitive to changes in vocal fold elongation (see Fig. 6). The experimental measurement data showed that nondirect glottal area component has a relative maximum near -5%. This is associated with the decreased stiffness of vocal folds at the negative elongation according to (10). With the increase of elongation, the vocal fold stiffness increases, and thus, the nondirect glottal area component decreases. In addition, nondirect component has a negative slope for elongations between 10% and 40%, and is zero for larger elongations. This is physiologically consistent, because sufficiently large elongations are known to inhibit phonation. The direct component $\bar{a}$ of glottal area data does not significantly change in large elongations. It is interesting to note that the theoretical and experimental direct components at 18-cm H_2O of subglottal pressure do not agree as good as 24-cm H_2O. A relatively large deviation of $\bar{a}$ can be found at negative elongations. This may be associated with more slack or low-stressed vocal folds at lower subglottal pressures and vocal fold elongations.

Vocal fold elongation is an important parameter to model and explore, as it is the main determinant of fundamental frequency. The anatagonistic actions of the cricothyroid and thyroarytenoid muscles comprise a frequency space such that increasing cricothyroid muscle activation tends to increase fundamental frequency and increasing thyroarytenoid muscle activity tends to decrease fundamental frequency. These muscles can be differentially affected by neurological disease; for example, recurrent laryngeal nerve paralysis affects thyroarytenoid muscle control while superior laryngeal nerve paralysis affects cricothyroid muscle control. More complicated diseases of muscle control, such as Parkinsonism and spasmodic dysphonia, also cause changes in the activation of these muscles. For example, Parkinsonism is characterized by a weak and breathy voice related to the bradykinesia, with vocal folds that are thin, bowed, and slightly abducted [22]. Modeling the effect of vocal fold elongation on voice has potential to elucidate and test the pathophysiological mechanisms of these diseases and how they affect voice. For example, both recurrent laryngeal nerve paralysis and superior laryngeal nerve paralysis could be simulated using the present model, and observations of the pathological models could be compared to *in vivo* observations. Vocal fold elongation and the glottal area time series can also be affected by pathologies that perturb the stiffness and elasticity of the vocal folds. Diseases such as Reinke's edema, vocal fold polyps, vocal fold nodules, laryngeal papillomatosis, and laryngeal cysts can all alter the rheological properties of the vocal fold cover and disrupt the sensitive relationship between vocal fold elongation and the direct and nondirect components of glottal area. Modeling normal voice as a function of vocal fold elongation is a key step in understanding the effect of these pathologies on the relationship between vocal fold elongation and glottal area waveform parameters.

V. Conclusion

In this paper, we introduced an extended model for simulating vocal fold elongation. The model was used to investigate the relationships between the direct and nondirect components of glottal area as a function of vocal fold elongation. Numerical results were calculated in this model, and compared to experimental results measured using high-speed imaging in 13 excised canine larynges. The average total power of the glottal area signal equals the sum of the powers of the direct and nondirect components. The nonmonotonic relationship between the nondirect component and vocal fold elongation suggests that there may be an optimal elongation to maximize the vocal fold vibratory power. In addition, an excessively large elongation inhibits vocal fold vibration. The model simulation showed a qualitative agreement with experimental high-speed imaging observations. The results suggest that this model is valuable in illustrating the effect of vocal fold elongation on certain measures of glottal area dynamics.

REFERENCES

[1] I. R. Titze, *Principles of voice production*. Englewood Cliffs, NJ: Prentice-Hall, 1994.

[2] L. C. Westphal and D. G. Childers, "Representation of glottal shape data for signal processing," *IEEE Trans. Acoust., Speech, Signal process.*, vol. 31, no. 3, pp. 766–769, Jun. 1983.

[3] J. Lohscheller, U. Eysholdt, H. Toy, and M. Dollinger, "Phonovibrography: Mapping high-speed movies of vocal fold vibrations into 2-D diagrams for visualizing and analyzing the underlying laryngeal dynamics," *IEEE Trans. Med. Imag.*, vol. 27, no. 3, pp. 300–309, Mar. 2008.

[4] Y. L. Yan, X. Chen, and D. Bless, "Automatic tracing of vocal-fold motion from high-speed digital images," *IEEE Trans. Biomed. Eng.*, vol. 53, no. 7, pp. 1394–1400, Jul. 2006.

[5] M. Dollinger, U. Hoppe, F. Hettlich, J. Lohscheller, S. Schuberth, and U. Eysholdt, "Vibration parameter extraction from endoscopic image series of the vocal folds," *IEEE Trans. Biomed. Eng.*, vol. 49, no. 8, pp. 773–781, Aug. 2002.

[6] C. Tao, Y. Zhang, and J. J. Jiang, "Extracting physiologically relevant parameters of vocal folds from high-speed video image series," *IEEE Trans. Biomed. Eng.*, vol. 54, no. 5, pp. 794–801, May 2007.

[7] R. Schwarz, U. Hoppe, M. Schuster, T. Wurzbacher, U. Eysholdt, and J. Lohscheller, "Classification of unilateral vocal fold paralysis by endoscopic digital high-speed recordings and inversion of a biomechanical model," *IEEE Trans. Biomed. Eng.*, vol. 53, no. 6, pp. 1099–1108, Jun. 2006.

[8] Y. Zhang and J. J. Jiang, "Spatiotemporal chaos in excised larynx vibrations," *Phys. Rev. E.*, vol. 72, pp. 35201–35204, 2005.

[9] K. Ishizaka and J.L. Flanagan, "Synthesis of voiced sounds from a two-mass model of the vocal cords," *Bell Syst. Tech. J.*, vol. 51, pp. 1233–1268, 1972.

[10] J. J. Jiang, Y. Zhang, and J. Stern, "Modeling of chaotic vibrations in symmetric vocal folds," *J. Acoust. Soc. Am.*, vol. 110, pp. 2120–2128, 2001.

[11] Y. Zhang and J. J. Jiang, "Chaotic vibrations of a vocal fold model with a unilateral polyp," *J. Acoust. Soc. Am.*, vol. 115, pp. 1266–1269, 2004.

[12] Y. Zhang, J. J. Jiang, and D. A. Rahn, "Studying vocal fold vibrations in Parkinson's disease with a nonlinear model," *Chaos*, vol. 15, p. 33903, 2005.

[13] F. Alipour and I. R. Titze, "Elastic models of vocal fold tissues," *J. Acoust. Soc. Am.*, vol. 90, pp. 1326–1331, 1991.

[14] A. Yang, J. Lohscheller, D. A. Berry, S. Becker, U. Eysholdt, D. Voigt, and M. Dollinger, "Biomechanical modeling of the three-dimensional aspects of human vocal fold dynamics," *J. Acoust. Soc. Am.*, vol. 127, pp. 1014–1031, 2010.

[15] I. R. Titze and B. H. Story, "Rules for controlling low-dimensional vocal fold models with muscle activation," *J. Acoust. Soc. Am.*, vol. 112, pp. 1064–1076, 2002.

[16] B. H. Story and I. R. Titze, "Voice simulation with a body cover model of the vocal fold," *J. Acoust. Soc. Am.*, vol. 97, pp. 1249–1260, 1995.

[17] Y. Zhang, J. J. Jiang, C. Tao, E. Bieging, and J. K. MacCallum, "Quantifying the complexity of excised larynx vibrations from high-speed imaging using spatiotemporal and nonlinear dynamic analyses," *Chaos*, vol. 17, p. 043114, 2007.

[18] Y. Zhang, E. Bieging, H. Tsui, and J. J Jiang, "Effective and efficient extraction of vocal fold vibratory patterns from high-speed digital imaging," *J. Voice*, vol. 24, pp. 21–29, 2010.

[19] C. Tao and J.J. Jiang, "A self-oscillating biophysical computer model of the elongated vocal fold," *Comput. Biol. Med.*, vol. 38, pp. 1211–1217, 2008.

[20] L. Bailly, N. Henrich, and X. Pelorson, "Vocal fold and ventricular fold vibration in period-doubling phonation: Physiological description and aerodynamic modeling," *J. Acoust. Soc. Am.*, vol. 127, no. 5, pp. 3212–3222, May 2010.

[21] T. Wurzbacher, M. Döllinger, R. Schwarz, U. Hoppe, U. Eysholdt, and J. Lohscheller, "Spatiotemporal classification of vocal fold dynamics by a multimass model comprising time-dependent parameters," *J. Acoust. Soc. Am.*, vol. 123, no. 4, pp. 2324–2334, Apr. 2008.

[22] G. Woodson, "Management of neurologic disorders of the larynx," *Ann. Otol Rhinol Laryngol*, vol. 117, no. 5, pp. 317–326, May 2008.

Yu Zhang received the Ph.D. degree in nonlinear acoustics from Nanjing University, Jiangsu, China.

He is currently a Professor of Underwater Acoustic Communication and Marine Information Technology Xiamen University, Xiamen, Fujian, China. His research interests include nonlinear dynamics and chaos theory, acoustics, ocean acoustics, biomedical imaging, and signal processing. His research also involves modeling chaotic vibrations of vocal folds and nonlinear time series analysis of biomedical systems. He has published more than 60 original papers in these areas.

Michael F. Regner received the B.A. degree from the University of Wisconsin-Madison School of Medicine and Public Health, Maidson, WI, where he is currently working toward the M.D. degree.

His research interests include excised scanine larynx modeling, mathematical modeling of vocal fold vibration, and voice aerodynamics. He has eight original papers in these areas.

Jack J. Jiang received the M.D. degree from Shanghai Medical University, Shanghai, China, in 1983, and the Ph.D. degree in speech pathology and audiology from the University of Iowa, Iowa City, in 1991.

He is currently a Professor in the Division of Otolaryngology and Biomedical Engineering, University of Wisconsin School of Medicine and Public Health, Madison. His current research endeavors focus on the vibratory properties of the vocal folds via studies of excised larynges, biomechanical modeling, aerodynamics, and analysis of laryngeal microstructure. He has more than 130 original publications in the area of voice measurement and disorders.